Composites Science and Technology 171 (2019) 244–251

Contents lists available at ScienceDirect

Composites Science and Technology

journal homepage: www.elsevier.com/locate/compscitech

Flexible and coatable insulating silica aerogel/polyurethane composites via soft segment control

Jaehyun Cho[a], Han Gyeol Jang[a,b], Seong Yun Kim[b,*], Beomjoo Yang[a,c,**]

[a] Institute of Advanced Composite Materials, Korea Institute of Science and Technology (KIST), 92 Chudong-ro, Bongdong-eup, Wanju-gun, Jeonbuk, 55324, Republic of Korea

[b] Department of Organic Materials and Fiber Engineering, Chonbuk National University, 567 Baekje-daero, Deokjin-gu, Jeonbuk, 54896, Republic of Korea

[c] School of Civil Engineering, Chungbuk National University, Chungdae-ro 1, Seowon-Gu, Cheongju, Chungbuk 28644, Republic of Korea

ARTICLE INFO

Keywords:
A. Polymer-matrix composites (PMCs)
B. Thermal properties
A. Coating
A. Flexible composites

ABSTRACT

We herein propose a facile approach to fabricate foldable and coatable silica aerogel polyurethane composites (APCs). For the flexibility control, the soft segment of polyurethane (PU) is manipulated. The change in soft segment length induces a difference in overall glass transition temperature of PU. When the silica aerogel content is increased, the PU with a shorter soft segment length shows brittle fracture behavior, while the PU with a longer soft segment length shows no breakage after bending. The thermal insulation properties of APCs were enhanced by 72% reduction in thermal conductivity upon 30 wt% aerogel loading and theoretically verified by a micromechanics-based thermal conductivity model considering the effects of interface and agglomeration. In addition, for the combustion behavior measurements, heat release rate and heat release capacity are substantially reduced for the APCs compared to neat PUs. Those enhanced thermal insulation properties may have a commercial impact on thermal insulation applications.

1. Introduction

Aerogels are highly porous and low-density materials, which make them extremely attractive in many application fields [1]. Aerogels were first reported in the 1930s by Kistler, who fabricated a highly porous three-dimensional network structure through a sol-gel process [2], and since then many types of aerogels have been investigated with different sources: silica [3,4], polymer [5,6], and transition metals [7]. As the most actively investigated aerogel since Kistler, silica aerogels have a high porosity (> 90%), a low density (0.003–0.1 g/cm^3), and a low thermal conductivity (0.013–0.14 W/m K) [8]. Due to those unique physical properties, silica aerogels have the full potential to be applied in aerospace-related fields, including thermal insulation panels [9,10], heat storage devices [11], and acoustic barriers [12,13], and etc. [14,15]. Other than silica aerogels, polymer-based aerogels are further pyrolyzed to form carbon aerogels [16], which have superior physical properties and are capable of being applied to capacitors [17], fuel storage devices [18], and catalyst supports [19]. Additionally, inorganic oxide aerogels based on transition metals are used for a variety of applications [7,20,21].

However, due to the fragile nature of the aerogels, durable aerogel composites assisted by other material over strengthening the aerogels themselves are mainly required for industrial purposes [22]. At the beginning, some groups attempted to increase the density of the aerogel itself to increase the mechanical strength while preserving the useful thermal insulation properties [23,24]. However, reinforcement by either increasing the density or adopting the aging process of silica aerogels was not enough for a wide range of aerospace applications [25,26]. As alternative methods of reinforcing silica aerogels, several approaches have been tried to bind an organic polymer to the silica aerogels [27–29] or to manipulate the interface between the silica gels and the polymers [30,31]. In addition, some groups have used fibers as a reinforcing filler material [32] or electrospun aerogel fiber webs [33–35] to increase flexibility. Although several approaches have shown effective mechanical reinforcements in silica aerogel composites, it is noteworthy, in fact, that most aerogel composites cannot be reshaped due to their brittleness under a large bending motion.

To overcome the brittleness of aerogel composites, we herein proposed a convenient approach to impregnate silica aerogel into a polymer matrix for maintaining the overall flexibility of the APCs. The APCs were fabricated through a simple two-step polymerization of PU and mixed with silica aerogel with preserved pores. Thermal

* Corresponding author.
** Corresponding author. School of Civil Engineering, Chungbuk National University, Chungdae-ro 1, Seowon-Gu, Cheongju, Chungbuk 28644, Republic of Korea.
E-mail addresses: sykim82@jbnu.ac.kr (S.Y. Kim), b.yang@chungbuk.ac.kr (B. Yang).

https://doi.org/10.1016/j.compscitech.2018.12.027
Received 8 October 2018; Received in revised form 16 December 2018; Accepted 23 December 2018
Available online 26 December 2018
0266-3538/

conductivity and pyrolysis combustion flow calorimetry (PCFC) analysis of the APCs clearly showed increased thermal insulation performance. We demonstrated the APCs as a heat insulating material with maintained foldability without breakage at certain PU compositions. In addition, enhanced thermal insulation performance of the APCs was achieved as a coating on substrates and was observed via visual images through an infrared (IR) camera. Finally, the correlation between the thermal insulation properties of silica aerogels and the overall thermal conductivity of the APCs was theoretically analyzed by micromechanical thermal conductivity modeling and compared with the experimental results.

From an industrial point of view, aerogel composite production costs and scale-up remain problematic. We believe the proposed APC fabrication process could be realized in broader application fields as it enables the APC material to be coated on substrates by manipulating the composite solution viscosity. With our suggested method of simultaneously modifying the flexibility and processability of aerogel composites according to our purpose, the resulting APCs may find new applications requiring both high thermal insulation and mechanical adjustability for various practical uses.

2. Methods

2.1. Materials

All solvents and reagents were used with molecular sieves for removing contained moisture. Poly(tetramethylene ether glycol) (PTMG) with three different molecular weights (M_n = 210, 650, and 1000 g/mol) were obtained from Korea PTG Co., Korea. 2,4-diphenylmethane diisocyanate (MDI) and 1–4 butanediol (BD) were obtained from Aldrich, USA. For faster chain extension reaction, dibutyltin dilaurate as a catalyst was obtained from Aldrich, USA. The silica aerogel powder with particle sizes between 1 and 10 μm and an average pore size of 20 nm was obtained from EM-POWER, Korea. Anhydrous dimethylformamide (DMF) and hexane were obtained from Aldrich, USA, and from Daejung Co., Korea, respectively.

2.2. Synthesis of silica aerogel filled PU composites

The polymerization was conducted in a 70-ml vial under inert conditions. First, MDI was placed in the vial in a 40 °C oil bath and purged with nitrogen gas. Keeping the vial in an inert atmosphere with the nitrogen gas, PTMG diluted with DMF solvent was gradually injected into the vial at a MDI to PTMG molar ratio of 2 to 1. Under continuous magnetic stirring at 200 rpm, the solution turned into a clear and viscous state, presumed to be the prepolymer, within 30 min. Once the solution became viscous, it was cooled down to room temperature; then, BD dissolved in DMF solvent as a chain extender was added dropwise into the solution. After 10 min of stirring, the polymer solution was further dried in an 80 °C convection oven for a day to complete the polymerization.

For the fabrication of silica aerogel impregnated PU composite, a solvent with low surface tension, hexane in this case, was dropped onto completely dried silica aerogel at a mass ratio of 1–2.5 for full wetting of the aerogel and to preserve the pore volume of the aerogel. As represented in Fig. S1, several solvents were used to find the best solvent for maximizing pore preservation with the greatest reduction in thermal conductivity. For composite fabrication, the PU solution prepared from the polymerization was mixed with the hexane-soaked silica aerogel from 5 to 30% in weight fraction. Once the mixture was mixed, it was spin-coated at 1500 rpm for 10 s using a spin-coater and then dried in an 80 °C convection oven for a day. The resulting thickness of the PU silica aerogel composite specimen ranged from 300 to 500 μm.

2.3. Characterization

All silica aerogel-impregnated PU composite films were fabricated by using a spin-coater machine (spin process controller, MIDAS, Daejeon, Korea). The surface functional groups of the PU films were analyzed in attenuated total reflection (ATR) mode using fourier transform-infrared spectroscopy (FT-IR, Nicolet 6700, Thermo Scientific, MA, USA). The molecular weight of the synthesized PU was measured by gel permeation chromatography (GPC, HLC-8320GPC, EcoSec, Japan) calibrated with a polystyrene standard. Tetrahydrofuran was used as the mobile phase for GPC analysis. Thermogravimetric analysis (TGA, Q50, TA Instruments, USA) was carried out to measure the decomposition temperature profile under nitrogen gas flow at a heating rate of 20 °C/min up to 600 °C. Differential scanning calorimetry (DSC, Q20a, TA Instruments, USA) was used to monitor changes in the glass transition temperature (T_g) of the composites with different silica aerogel fractions. For the DSC measurements, the samples were heated at a rate of 10 °C/min from −50 to 200 °C and cooled at a rate of 10 °C/min from 200 to −50 °C under a nitrogen atmosphere. Dynamic mechanical analysis (DMA, Q800, TA Instruments, USA) measurement of the APC films (30 mm length, 5 mm wide, and ca. 30 μm thickness) was conducted in air at a heating rate of 3 °C/min with a load frequency of 1 Hz. Morphological analysis of the composites was conducted using two different methods. First, scanning electron microscopy (SEM, Nova NanoSEM 450, FEI Corp., USA) with X-ray energy-dispersive spectroscopy (EDS, FEI Verios 460 L, FEI Corp., USA) was used to observe the dispersion state of the silica aerogel powder inside the PU film. To prepare the specimens for measurement, the samples were fractured under liquid nitrogen and sputter-coated with platinum for 120 s in vacuum using a sputter-coating machine (Ion Sputter E-1030, Hitachi High Technologies, Japan). Second, micro-computed tomography (m-CT, SkyScan 1172, Bruker Co., USA) was used to identify the dispersion and network structures of the silica aerogels in the composites. The thermal conductivity of the composites was monitored according to the ISO 22007-2 standard (TPS 2500S, Hot Disk AB, Sweden). PCFC measurements were carried out with a micro-calorimeter (FAA Micro Calorimeter, Fire Testing Technology Ltd., UK). Samples were heated to 900 °C at a constant heating rate of 1 °C/s in a stabilized atmosphere (at an oxygen flowrate of 20 cm^3/min and a nitrogen flowrate of 80 cm^3/min). Thermal IR images of the samples were observed by a thermal imaging camera (Testo, 875-1i), by placing the samples on top of aluminum foil covered surface of heating plate. The APC coated side is faced down to the heating plate to insulate the thermal energy transfer from the heat source.

2.4. Theoretical framework

Let us start by considering the PU matrix (phase 0) and the randomly distributed aerogel particles (phase 1) with the interface of Kapitsa resistance (R_K). A schematic illustration of the composite is shown in Fig. 1a, assuming that aerogels are coated with a thin interface layer. The constitutive thermal model proposed in preceding work [36], which considered the interface effect, is extended to predict the insulation properties of composites containing particle-shaped aerogels. Based on the ensemble volume averaged method [37], the effective thermal conductivity $\mathbf{K}^*$ for two-phase composites can be written as:

$$\mathbf{K}^* = \mathbf{K}_0 \cdot [\mathbf{I} + \phi_1(\mathbf{S} - \mathbf{A}_1)^{-1} \cdot \{\mathbf{I} - \phi_1 \mathbf{S} \cdot (\mathbf{S} + \mathbf{A}_1)^{-1}\}]^{-1} \quad (1)$$

where $\mathbf{K}_q$ and ϕ_q are the thermal conductivity and volume fraction of the q-phase, $\mathbf{I}$ denotes an identical tensor, $\mathbf{S}$ signifies Eshelby's tensor, and, when the shape of the inclusions is spherical, $\mathbf{S}$ is defined as: $S_{11} = S_{22} = S_{33} = 1/3$.

$\mathbf{A}_1$ can be defined as: $\mathbf{A}_1 = \{(\mathbf{K}_1)^i - \mathbf{K}_0\}^{-1} \cdot \mathbf{K}_0 \cdot \Psi$, where the superscript i denotes the interface and Ψ signifies the agglomeration constant. The thermal conductivity of spherical particles considering the Kapitsa resistance ($(\mathbf{K}_1)^i$) can be expressed as follows [38].

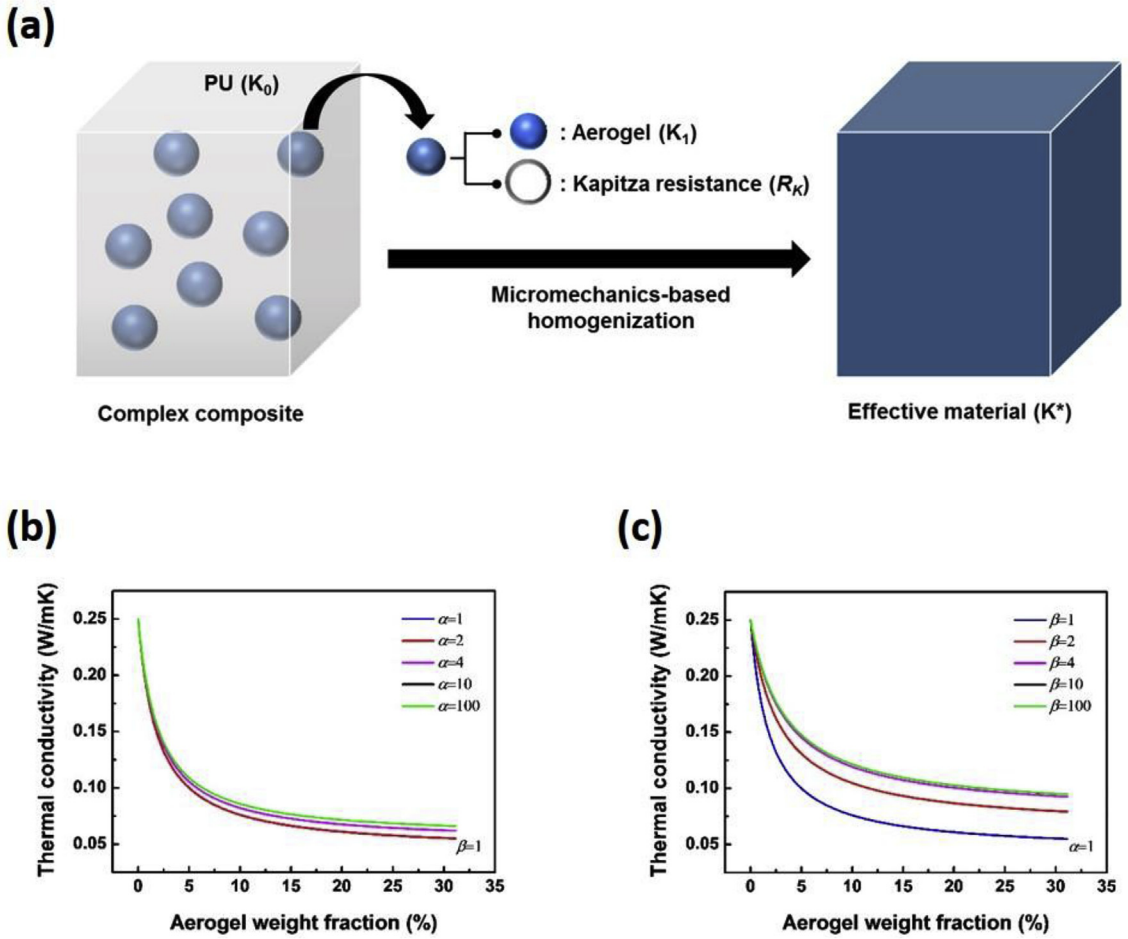

Fig. 1. (a) Theoretical illustration of spherical aerogel-embedded PU composites and the influences of the model parameters related to (b) the Kapitza interface and (c) inclusion agglomeration on the overall thermal conductivity of APC.

$$(\mathbf{K}_1)^i = \frac{d\mathbf{K}_1}{d + 2(R_K)\mathbf{K}_1} \tag{2}$$

where R_K denotes the Kapitsa resistance defined as $10^{-\alpha}$, d is the diameter of the filler, and α is the first model parameter for the interface between PU and the aerogel materials. In addition, since a very large quantity of aerogels is incorporated into the matrix, the effect of agglomeration (Ψ) should be considered. Herein, it is assumed that the damping effect due to filler agglomeration is modeled via the logistic cumulative distribution function as follows.

$$\Psi = 0.5 + \frac{e^{\beta}}{1 + e^{\beta}} \tag{3}$$

where β is the second model parameter for filler agglomeration.

A series of parametric studies are conducted, and the results are plotted in Fig. 1b and c to elucidate the potential of the proposed model. The material constants adopted in the parametric simulation are as follows: $\mathbf{K}_0 = 0.250$ W/m K, $\mathbf{K}_1 = 0.015$ W/m K, $d = 5$ μm. It can be seen in Fig. 1b that thermal conductivity becomes higher as R_K continues to increase. However, as α becomes larger, the interface effect gradually decreases and converges to a specific value. This signifies the maximum-minimum boundary that can be controlled by the interface. In Fig. 1c, it can be observed that the effect of filler agglomeration is more pronounced as the parameter β increases. The agglomeration effect also converges to a specific value, and it signifies the different maximum-minimum boundary that is influenced by the dispersion of inclusions. The dispersion-dependent agglomeration effect may be available when the content of inclusions is very high and exceeds 50% by volume. When the agglomeration effect is not needed to be considered, the parameter β should be fixed at zero.

3. Results and discussion

3.1. Synthesis of APCs

Prior to APC fabrication, PU was synthesized by a typical two-step polymerization method [39], i.e., the prepolymer method, as shown in Fig. 2. First, isocyanate-terminated prepolymers were synthesized by reacting with two monomers, PTMG and MDI. In this step, the number average molecular weight (M_n) of PTMG (M_n = 210, 650, and 1000) was varied to control the flexibility of the polymer. Next, the prepared isocyanate-terminated PTMGs were chain-extended with BD to achieve a uniform and narrow distribution, which was the advantage of the prepolymer method. According to the type of PTMG used, the PUs were named after the number average molecular weight of PTMG, i.e., PU210, PU650, PU1000, and the corresponding number and weight average molecular weights and polydispersity index (PDI) of the PUs are summarized in Table 1. At the end of the polymerization process, the silica aerogels with pores preserved by presoaked hexane were added to the PU solution with DMF. The premixture was spin-coated and cured in a convection oven to fabricate the APCs.

The synthesized PUs were confirmed by FT-IR and GPC. Fig. S2a shows the FT-IR spectra for the characteristic peaks of PU, PU prepolymer, silica aerogels, and their composites. At the first step of the prepolymer formation, the corresponding characteristic peak of the N=C=O group is represented at approximately 2400 cm^{-1}. After completion of the polymerization, the characteristic peaks of PUs were

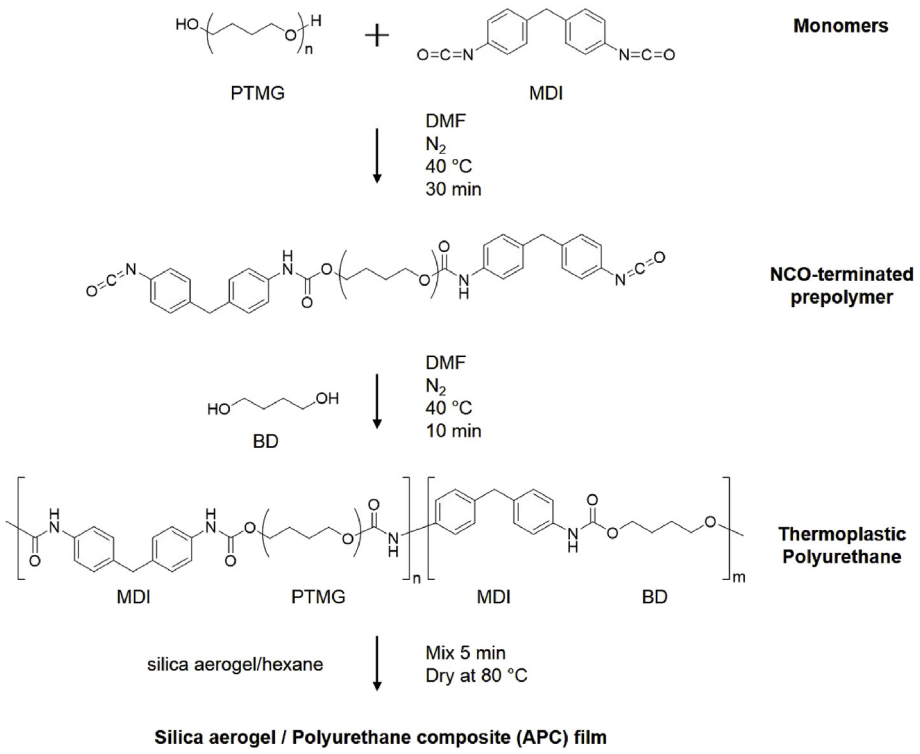

Fig. 2. Schematic of PU synthesis and fabrication process of APC.

observed [39]: the absorption peak at approximately 3300 cm^{-1} for N—H and 1690 cm^{-1} for C═O, both from the urethane linkage. In addition, both the disappearance of the absorption peak for the N═C═O group and the appearance of the N—H absorption peak suggest that PU was successfully synthesized. It is also noteworthy that the extent of hydrogen bonding affected by the monomer composition can be traced by monitoring the carbonyl bond shift. In the FT-IR spectra, the absorption peak at approximately 1730 cm^{-1}, corresponding to free C═O, shifted to approximately 1700 cm^{-1}, corresponding to H-bonded C═O, as the molecular weight of PTMG decreased [40]. In other words, when the fraction of the long and flexible segment, PTMG, decreases with the number average molecular weight, there are more extensive intermolecular interactions among the hard segments. For all APCs, the representative peaks were shown as broad peaks at approximately 1020 and 1090 cm^{-1}, which represent the characteristic peaks of silica aerogel: 3500 cm^{-1} for O—H and 1100 cm^{-1} for bending stretch of Si—O—Si [41]. Fig. S2b shows the comparison between the GPC traces of PU210, PU650 and PU1000. In all PUs, a high molecular weight was obtained, indicating that PU synthesis was successfully performed. The corresponding values for the number-average molecular weights (M_n), the weight-average molecular weights (M_w), and the molecular weight distributions (M_w/M_n) are summarized in Table 1. The molecular weight data suggest that no apparent molecular weight difference was observed in any of the samples, which have narrow PDI values.

3.2. Morphology

Fig. 3 summarizes the morphological analysis of the PU1000 series. Fig. 3a shows a demonstration of coating process of APC solution on a substrate. As revealed in Fig. 3a, the resulting APC layer shows translucent property when coated. Fig. 3b demonstrates the flexibility and stretchability of resulting APC films. It was clearly observed that after twisted, stretched, and bent, the film still retain its original shape without breakage. (Fig. S3 shows the images of APC films in different PU compositions with 30 wt% silica aerogel). All APC films had a translucent property due to the presence of silica aerogel. In Fig. S3, when the film was bent, PU1000-30 and PU650-30 showed flexible properties, while PU210-30 had a crack on the edge of the film from the bending motion. It was found that flexible APCs with 30 wt% silica aerogel were successfully fabricated using PU1000 and PU650. However, at higher silica aerogel contents above 30 wt% of the silica aerogel, even the PU1000 and PU650 films showed brittle fracture from the bending motion.

As shown in Fig. 3c, m-CT analysis was performed for the non-destructive visualization of aerogel distribution on PU1000-30. Although the pore size of the aerogel itself could not be measured due to the resolution limitation of the equipment, the different aerogel contents and general scope of distribution were observed. As the silica aerogel content increase from 0 to 30 wt%, the volume of white spots

Table 1
The composition, measured molecular weight parameters and PDI of synthesized PUs and APCs.

Sample Code		Mole Ratio			MW of PTMG (g/mol)	Silica aerogel content (wt %)	M_n (g/mol)	M_w (g/mol)	PDI (M_w/M_n)	Bulk Density (g/mL)
		PTMG	MDI	BD						
Neat PU	PU210	1	2	1	210	0	17515	40106	2.29	1.249
	PU650	1	2	1	650	0	25920	53228	2.05	1.180
	PU1000	1	2	1	1000	0	16627	38971	2.34	1.042
APC	PU1000-15	1	2	1	1000	15				0.710
	PU1000-30	1	2	1	1000	30				0.580

*M_w: weight average molecular weight.

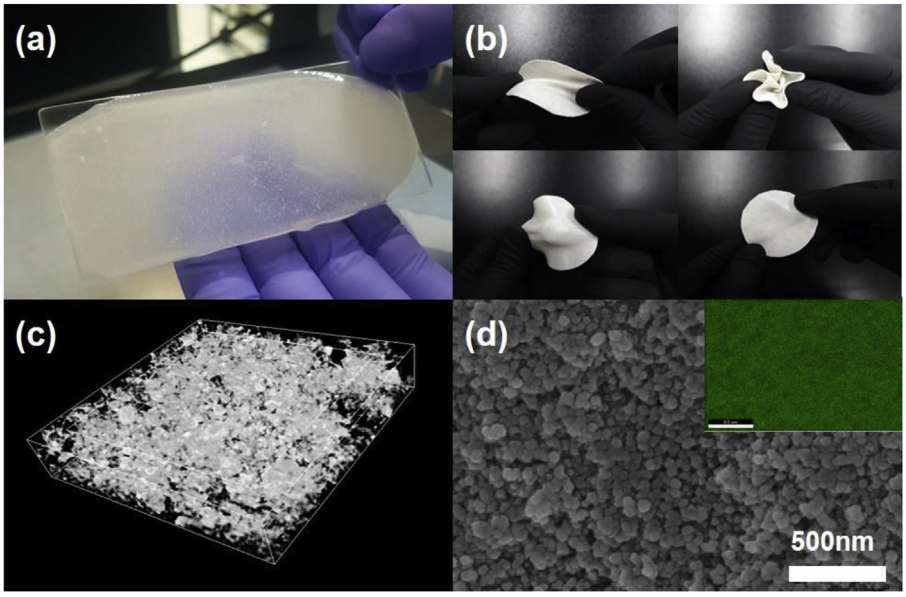

Fig. 3. The photographs of (a) coated APC (PU1000-30) on a substrate and (b) twisting, stretching, and bending test of APC film (PU1000-30). Morphology analysis of APC (PU1000-30): (c) m-CT image and (d) SEM image with EDS mapping image for Si as an inset.

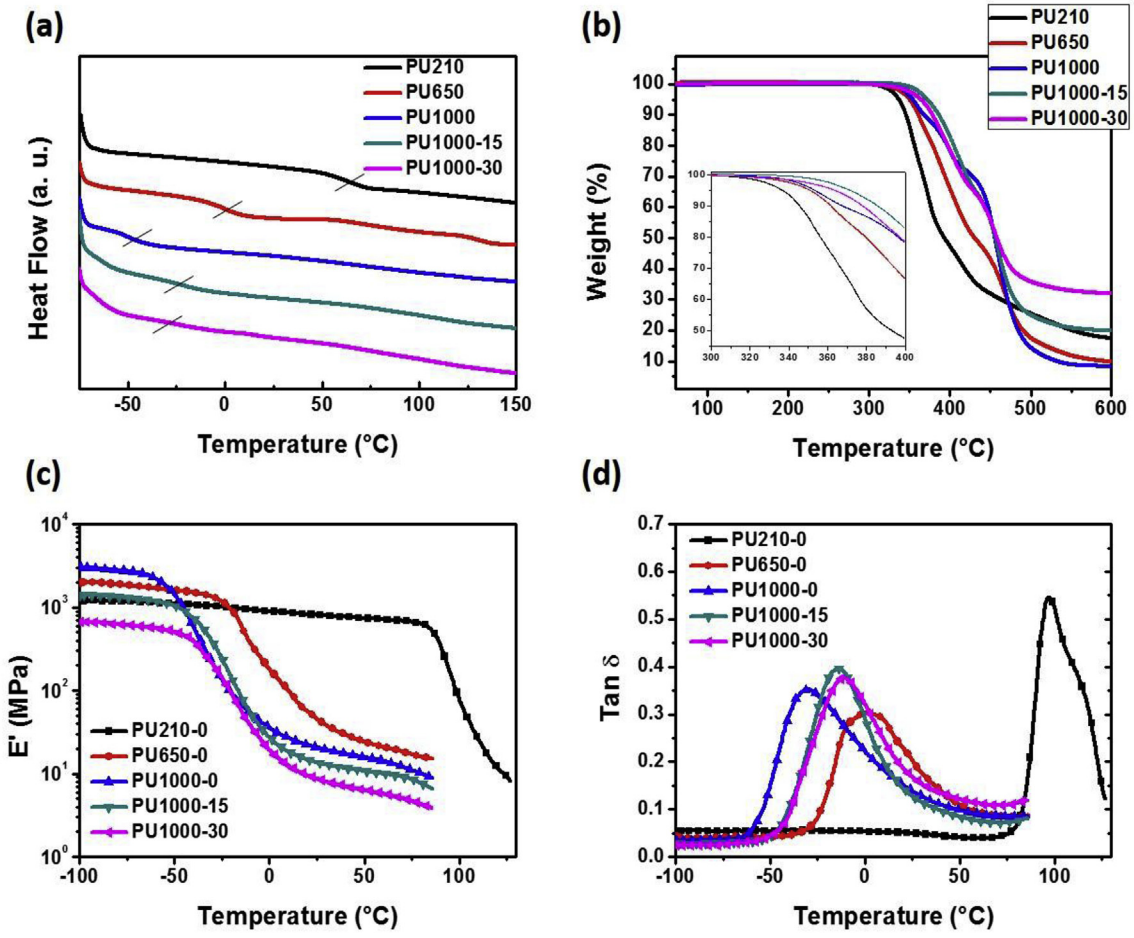

Fig. 4. Thermal properties of the neat PUs and APCs: (a) DSC curves, (b) TGA curves. (Inset: enlarged view of TGA curves from 300 to 400 °C); DMA curves of the neat PUs and APCs: (c) Storage modulus, (d) Tan δ.

Table 2
The glass transition temperature (T_g), thermal decomposition temperatures ($T_{5\%}$ and $T_{30\%}$), heat-resistance index and char yield of the PUs and APCs.

Sample Code	T_g (°C)		$T_{5\%}$	$T_{30\%}$	Heat-resistance index	Char yield (%)
	DSC	DMA				
PU210	68.0	97.4	336.6	366.7	173.8	16.6
PU650	−7.0	1.1	350.9	394.7	184.8	8.9
PU1000	−47.0	−30.4	353.7	428.2	195.2	8.4
PU1000-15	−25.0	−14.2	371.7	421.0	196.6	19.4
PU1000-30	−27.4	−11.0	363.9	415.9	193.6	31.6

on the image was increased (Fig. S4). Fig. 3d shows the SEM image of the fracture surface and corresponding elemental analysis to detect the distribution of silica aerogel inside the composite. A network of silica aerogel particles inside the flexible matrix and corresponding EDS mapping image (inset of Fig. 3d) of Si also confirms the homogeneous distribution of silica aerogel at 30% loading. The distribution of silica aerogel network and fracture surfaces of APCs can be seen in Figs. S5 and S6.

3.3. Thermal properties of APCs

The thermal properties of PUs and APCs were characterized by DSC, TGA and DMA. Fig. 4a shows DSC curves for PU210, PU650, PU1000 and silica aerogel containing PU1000s (PU1000 series). The T_g changed with the length of PTMG at the same molar ratio of monomers. As analyzed from the FT-IR graph (Fig. S2a), PU1000 has weaker intermolecular interactions due to the longer length of PTMG, leading to the lowest T_g of the pristine PU series. Compared to PU210, of which the T_g is 68.0 °C, PU 650 and PU1000 showed much lower T_g values of −7.0 °C and −47.0 °C, respectively. In other words, the higher the molecular weight of PTMG, the more flexible the synthesized PU was. Additionally, for the APCs, T_g of PU1000 was increased from −47.0 °C to −25.0 °C and −27.4 °C for PU1000-15 and PU1000-30, respectively. The corresponding data are given in Table 2.

Fig. 4b shows TGA curves for the pristine PUs and APCs. The TGA curves of PUs showed multistep degradation since both the hard segment and soft segment dissociate at different temperatures [42,43]. The first stage of the decomposition temperature (between $T_{5\%}$ and $T_{10\%}$) is attributed to the dissociation of hard segments, that is, urethane bonds. In the second stage, the thermal decomposition of soft segments of PU took place with a mass loss around $T_{30\%}$. The measured residual weights and heat resistance indices for all samples are given in Table 2 and Fig. S7. The corresponding heat-resistance indices were calculated by following the equation [44]:

$$T_{heat-resistance\ index} = 0.49 \times [T_{5\%} + 0.6 \times (T_{30\%} - T_{5\%})] \quad (4)$$

where $T_{5\%}$ and $T_{30\%}$ are the decomposition temperatures at which there is a 5% and 30% weight loss, respectively. The results of the increased heat resistance index suggest that the thermal stability of pristine PU1000 as well as silica aerogel-added PU1000 is higher than that of PU210 and PU650.

As shown in Fig. 4c and d, the DMA measurements were carried out to prove the temperature dependent storage modulus of the APCs and the effect of silica aerogels on the flexibility of the PU1000 composites, respectively. Fig. 4c displays the storage modulus of the PUs and PU1000 composites as a function of temperature. An effective decrease in the storage modulus of PU210, PU650 and PU1000 was observed at 97.4 °C, 1.1 °C and −30.4 °C, respectively. For the PU1000 composites with varying aerogel contents, the storage moduli of each of the composites were not clearly differentiated within the temperature range. However, since the storage modulus of PU1000 starts to rapidly drop at earlier stage of heating, compared to the outcomes with PU650 and PU210, the PU1000 is more flexible among these PU compositions and is also more suitable for coating process over PU650 and PU210. Fig. 4d represents the tan δ for the pristine PUs and PU1000 composites. Since the tan δ peak values represent the T_g, it was clearly revealed that PU1000 has the lowest T_g, which means PU1000 is more flexible than PU210 or PU650. For the PU1000 composites, T_g was increased as silica aerogel was added, which may be ascribe to the interruption of polymer chain movement caused by the incorporation of aerogel particles. In addtion, comparing the PU1000-15, there was slight increment in T_g of PU1000-30, and this represents spatially particular dispersion of the aerogels due to high volumetric occupation [45]. Based on the comparison of T_g values measured by DSC and DMA, although absolute T_g values are dependent on sample preparation and detecting methods, the trend in the T_g values was cross-checked [46].

3.4. Thermal insulation properties of APCs

So far, it has been demonstrated that the flexibility of APCs is retained even with 30 wt% of silica aerogel impregnation and improved thermal properties. To monitor more direct information of thermal insulation properties of the APCs due to the introduction of silica aerogel, thermal conductivity was measured, and the analytical prediction for the effective thermal characteristics of the insulating composites are shown in Fig. 5a. For the experimental values, all APC films were measured for through-plane thermal conductivity. The pristine PU films

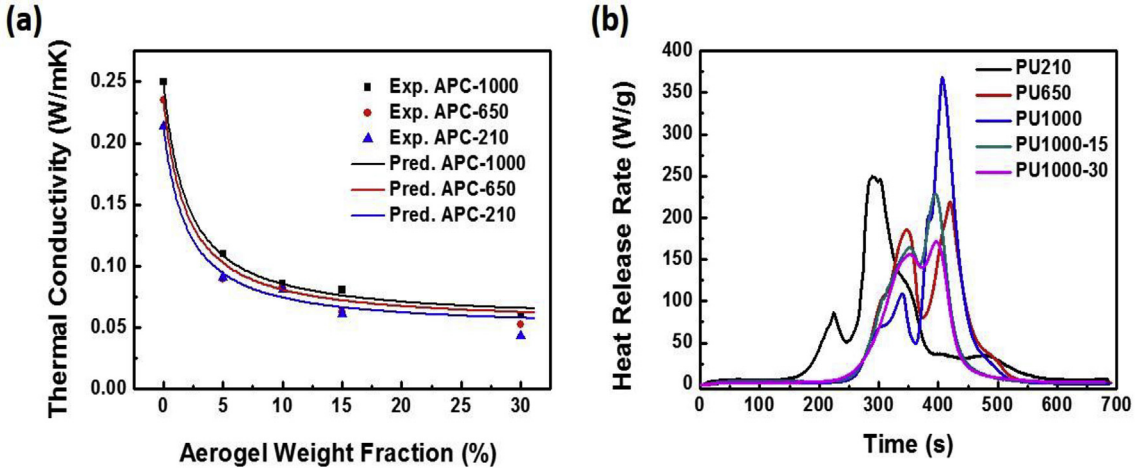

Fig. 5. Thermal insulation properties of the APCs: (a) Comparison of thermal conductivity measured by the experiments and calculated with correlated theories, (b) PCFC analysis of the APCs.

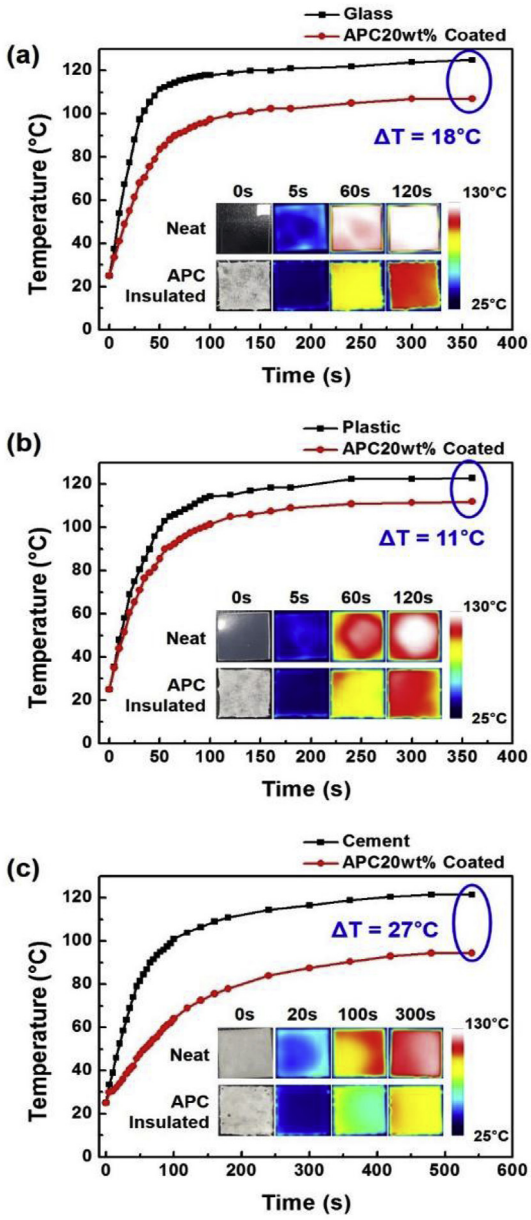

Fig. 6. Temperature profiles of (a) glass and APC coated glass, (b) polypropylene and APC coated polypropylene, and (c) cement and APC coated cement as a function of time on setting temperature at 130 °C. The inset represents the thermal IR images of neat samples and APC insulated samples from top to bottom, respectively, and increasing heating time from left to right, respectively.

showed a relatively high thermal conductivity in the range of 0.252 to 0.214 W/m K. As the silica aerogel content in the APC increased, the thermal conductivity decreased. At 30 wt% silica aerogel, the thermal conductivity decreased to the range of 0.066 to 0.043 W/m K, which represents a 74–80% reduction in thermal conductivity.

In addition, the micromechanics-based thermal conductivity prediction was compared with the experimental measurements. Since the model parameters of the simulation are difficult to obtain experimentally, they were computationally derived using a genetic algorithm by comparing the experimental results with the micromechanical predictions [47]. The fitted parameters for the present APCs are $\alpha = 5$ and $\beta = 1$, and the same values are applied to all cases regardless of the aerogel filler contents. The calculated predictions are in good agreement with the experimental results. It can be seen that the prediction does not fit well when 30% or more filler is incorporated into the PU matrix. This is because too much filler is incorporated into the resin (the weight fraction of 30% is approximately equal to the volume fraction of 90%), and thus additional consideration of filler interaction is required to accurately simulate. This problem is beyond the scope of the present study but will be considered in future studies.

In order to investigate the impact of this facile and scalable approach of producing thermal insulating composite material on practical application, the PCFC of the APCs are measured. PCFC is a technology developed in cooperation with the Federal Aviation Administration to measure the heat release rate (HRR) and heat release capacity (HRC) for evaluating the fire-resistant properties of polymer materials [48,49]. As shown in Fig. 5b and Fig. S8, and Table S1, compared to neat PUs, both the peak HRR and HRC were reduced in all APCs as the silica aerogel content increased. Since it is known that a lower HRC value indicates superior fire-resistant property, all APCs with 30% silica aerogel lie in the range of 'moderate fire resistance' [48]. Moreover, as shown in Fig. 5b, while the PU210 and PU650 series only showed a marginal reduction in both the HRR and the HRC as silica aerogel content increased, the PU1000 series showed the most reduction in fire-resistant properties.

For a practical application, APCs were coated on different substrates such as glass, plastic (polypropylene in this study), and cement that are widely used in industry. The APCs were coated as an insulating layer in 0.3 mm thickness and its coating process is presented as movie in Supplementary data. Fig. 6 shows the temperature profile of each sample (neat materials and APC coated materials) as a function of time while each sample is heated to 130 °C. As shown in Fig. 6, glass reached the steady state temperature the fastest among three materials and plastic and cement were heated slower than glass, including the APC coated samples. Although there was difference in temperature increasing speed among different materials, when reached its maximum temperature, i.e., steady state temperature, the average temperature difference between the neat sample and APC insulated sample was 18.7 °C with only 0.3 mm thickness of APC insulation layer. Since the each thickness of glass and plastic was 1 mm, assuming the total thickness difference between the neat sample and APC coated sample is 0.3 mm of APC layer, the effectiveness of thermal insulation was able to be estimated by changing the insulation layer thickness or aerogel content. In addition, assuming the thermal conductivity of the Portland cement was in near range of thermal conductivity of glass, as the thickness of cement is doubled by the thickness of glass, i.e., 2 mm, the temperature difference between the neat and APC coated samples became greater as 27 °C when reached steady state temperature. In other words, with only 0.3 mm thick of APC layer, the thermal insulation can be optimized by changing the material thickness. This experiment thus highlights our APC can be widely applied for industry purpose for efficient heat insulation.

Supplementary video related to this article can be found at https://doi.org/10.1016/j.compscitech.2018.12.027.

4. Conclusion

In summary, different series of PU elastomers were synthesized to control the flexibility of the composite. With different types of monomers, soft segment lengths were manipulated, and the resulting flexibility of the APCs was controlled enough to bear bending motion. Since silica aerogels have a high porosity, which would improve the thermal insulation properties of the APCs, processing method to preserve the pores of the aerogels was adopted. Hexane was found to be the best option to preserve the pores and maximize the thermal insulation properties. PU1000 had the greatest flexibility compared to the other series of PUs, i.e., PU210 and PU650, and flexibility was retained at 30 wt% silica aerogel content. For the thermal insulating properties, not only did the through-plane thermal conductivity of APCs decrease to the range of 0.066 to 0.043 W/m K, assuming the pores of the aerogels

were successfully preserved, but the HRR was also substantially reduced with a 30% silica aerogel content for the PU1000 series. As a practical application, 0.3 mm thick APCs were coated on several substrates, such as a glass, plastic, and cement, to observe the thermal insulation properties via an IR camera. The micromechanics-based thermal conductivity model was proposed to predict the effective thermal characteristics of insulating composites. The enhanced thermal insulation properties were theoretically verified by the proposed model.

Conflicts of interest

The authors declare no competing interest.

Acknowledgements

We acknowledge the financial support from a Korea Institute of Science and Technology internal project. This research was supported by Basic Science Research Program (2017R1C1B5077037) through the National Research Foundation of Korea (NRF) funded by the Ministry of Education and the Industrial Technology Innovation Program (10082586) Funded by the Ministry of Trade, Industry & Energy of Korea.

Appendix A. Supplementary data

Supplementary data to this article can be found online at https://doi.org/10.1016/j.compscitech.2018.12.027.

References

[1] A.C. Pierre, G.M. Pajonk, Chemistry of aerogels and their applications, Chem. Rev. 102 (11) (2002) 4243–4266.
[2] S.S. Kistler, Coherent expanded aerogels and jellies, Nature 127 (1931) 741.
[3] G. Zhang, A. Dass, A.-M.M. Rawashdeh, J. Thomas, J.A. Counsil, C. Sotiriou-Leventis, E.F. Fabrizio, F. Ilhan, P. Vassilaras, D.A. Scheiman, L. McCorkle, A. Palczer, J.C. Johnston, M.A. Meador, N. Leventis, Isocyanate-crosslinked silica aerogel monoliths: preparation and characterization, J. Non-Cryst. Solids 350 (2004) 152–164.
[4] H. Maleki, L. Durães, A. Portugal, An overview on silica aerogels synthesis and different mechanical reinforcing strategies, J. Non-Cryst. Solids 385 (2014) 55–74.
[5] S. Cardea, A. Gugliuzza, M. Sessa, M.C. Aceto, E. Drioli, E. Reverchon, Supercritical gel drying: a powerful tool for tailoring symmetric porous PVDF – HFP membranes, ACS Appl. Mater. Interfaces 1 (1) (2009) 171–180.
[6] C. Daniel, S. Giudice, G. Guerra, Syndiotactic polystyrene aerogels with β, γ, and ε crystalline phases, Chem. Mater. 21 (6) (2009) 1028–1034.
[7] N. Leventis, P. Vassilaras, E.F. Fabrizio, A. Dass, Polymer nanoencapsulated rare earth aerogels: chemically complex but stoichiometrically similar core-shell superstructures with skeletal properties of pure compounds, J. Mater. Chem. 17 (15) (2007) 1502–1508.
[8] H.M. Kim, Y.J. Noh, J. Yu, S.Y. Kim, J.R. Youn, Silica aerogel/polyvinyl alcohol (PVA) insulation composites with preserved aerogel pores using interfaces between the superhydrophobic aerogel and hydrophilic PVA solution, Composites, Part A 75 (2015) 39–45.
[9] M. Reim, W. Körner, J. Manara, S. Korder, M. Arduini-Schuster, H.P. Ebert, J. Fricke, Silica aerogel granulate material for thermal insulation and daylighting, Sol. Energy 79 (2) (2005) 131–139.
[10] B.P. Jelle, Traditional, state-of-the-art and future thermal building insulation materials and solutions – properties, requirements and possibilities, Energ. Buildings 43 (10) (2011) 2549–2563.
[11] J. Fricke, A. Emmerling, Aerogels—recent progress in production techniques and novel applications, J. Sol-Gel Sci. Technol. 13 (1) (1998) 299–303.
[12] R. Gerlach, O. Kraus, J. Fricke, P.C. Eccardt, N. Kroemer, V. Magori, Modified SiO2 aerogels as acoustic impedance matching layers in ultrasonic devices, J. Non-Cryst. Solids 145 (1992) 227–232.
[13] C.A. Morris, M.L. Anderson, R.M. Stroud, C.I. Merzbacher, D.R. Rolison, Silica sol as a nanoglue: flexible synthesis of composite aerogels, Science 284 (5414) (1999) 622–624.
[14] L.W. Hrubesh, Aerogel applications, J. Non-Cryst. Solids 225 (1998) 335–342.
[15] C.-T. Wang, C.-L. Wu, I.C. Chen, Y.-H. Huang, Humidity sensors based on silica nanoparticle aerogel thin films, Sens. Actuators, B 107 (1) (2005) 402–410.
[16] S. Haiyan, X. Zhen, G. Chao, Multifunctional, ultra-flyweight, synergistically assembled carbon aerogels, Adv. Mater. 25 (18) (2013) 2554–2560.
[17] B. Fang, L. Binder, A modified activated carbon aerogel for high-energy storage in electric double layer capacitors, J. Power Sources 163 (1) (2006) 616–622.
[18] A.S. Aricò, P. Bruce, B. Scrosati, J.-M. Tarascon, W. van Schalkwijk, Nanostructured materials for advanced energy conversion and storage devices, Nat. Mater. 4 (2005) 366.
[19] E. Guilminot, F. Fischer, M. Chatenet, A. Rigacci, S. Berthon-Fabry, P. Achard, E. Chainet, Use of cellulose-based carbon aerogels as catalyst support for PEM fuel cell electrodes: electrochemical characterization, J. Power Sources 166 (1) (2007) 104–111.
[20] J. Walendziewski, M. Stolarski, Synthesis and properties of alumina aerogels (II), React. Kinet. Catal. Lett. 71 (2) (2000) 201–207.
[21] H. Li, L. Song, Y. Fu, Y. Wei, R. Li, H. Liu, Loads transfer across static electrical phase interfaces in silica aerogel/polymethyl methacrylate composites, Compos. Sci. Technol. 138 (2017) 169–178.
[22] J.P. Randall, M.A.B. Meador, S.C. Jana, Tailoring mechanical properties of aerogels for aerospace applications, ACS Appl. Mater. Interfaces 3 (3) (2011) 613–626.
[23] J. Fricke, Aerogels — highly tenuous solids with fascinating properties, J. Non-Cryst. Solids 100 (1) (1988) 169–173.
[24] N. Leventis, C. Sotiriou-Leventis, G. Zhang, A.-M.M. Rawashdeh, Nanoengineering strong silica aerogels, Nano Lett 2 (9) (2002) 957–960.
[25] M.R. Miner, B. Hosticka, P.M. Norris, The effects of ambient humidity on the mechanical properties and surface chemistry of hygroscopic silica aerogel, J. Non-Cryst. Solids 350 (2004) 285–289.
[26] H. Sai, R. Fu, J. Xiang, Y. Guan, F. Zhang, Fabrication of elastic silica-bacterial cellulose composite aerogels with nanoscale interpenetrating network by ultrafast evaporative drying, Compos. Sci. Technol. 155 (2018) 72–80.
[27] M. Schmidt, F. Schwertfeger, Applications for silica aerogel products, J. Non-Cryst. Solids 225 (1998) 364–368.
[28] D.B. Mahadik, H.-N.-R. Jung, W. Han, H.H. Cho, H.-H. Park, Flexible, elastic, and superhydrophobic silica-polymer composite aerogels by high internal phase emulsion process, Compos. Sci. Technol. 147 (2017) 45–51.
[29] H.S. Kim, J.-u. Jang, H. Lee, S.Y. Kim, S.H. Kim, J. Kim, Y.C. Jung, B.J. Yang, Thermal management in polymer composites: a review of physical and structural parameters, Adv. Eng. Mater. 20 (10) (2018) 1800204.
[30] H. Maleki, L. Duraes, A. Portugal, Synthesis of mechanically reinforced silica aerogels via surface-initiated reversible addition-fragmentation chain transfer (RAFT) polymerization, J. Mater. Chem. A 3 (4) (2015) 1594–1600.
[31] M. Kim, K. Eo, H.J. Lim, Y.K. Kwon, Low shrinkage, mechanically strong polyimide hybrid aerogels containing hollow mesoporous silica nanospheres, Compos. Sci. Technol. 165 (2018) 355–361.
[32] Z. Li, L. Gong, X. Cheng, S. He, C. Li, H. Zhang, Flexible silica aerogel composites strengthened with aramid fibers and their thermal behavior, Mater. Des. 99 (2016) 349–355.
[33] H. Wu, Y. Chen, Q. Chen, Y. Ding, X. Zhou, H. Gao, Synthesis of flexible aerogel composites reinforced with electrospun nanofibers and microparticles for thermal insulation, J. Nanomater. 2013 (2013) 8.
[34] S. He, G. Sun, X. Cheng, H. Dai, X. Chen, Nanoporous SiO2 grafted aramid fibers with low thermal conductivity, Compos. Sci. Technol. 146 (2017) 91–98.
[35] Y.-G. Kim, H.S. Kim, S.M. Jo, S.Y. Kim, B.J. Yang, J. Cho, S. Lee, J.E. Cha, Thermally insulating, fire-retardant, smokeless and flexible polyvinylidene fluoride nanofibers filled with silica aerogels, Chem. Eng. J. 351 (2018) 473–481.
[36] S.Y. Kim, H.G. Jang, C.-M. Yang, B.J. Yang, Multiscale prediction of thermal conductivity for nanocomposites containing crumpled carbon nanofillers with interfacial characteristics, Compos. Sci. Technol. 155 (2018) 169–176.
[37] J.W. Ju, T.M. Chen, Effective elastic moduli of two-phase composites containing randomly dispersed spherical inhomogeneities, Acta Mech 103 (1) (1994) 123–144.
[38] C.-W. Nan, G. Liu, Y. Lin, M. Li, Interface effect on thermal conductivity of carbon nanotube composites, Appl. Phys. Lett. 85 (16) (2004) 3549–3551.
[39] C.K. Lee, D.A. Davis, S.R. White, J.S. Moore, N.R. Sottos, P.V. Braun, Force-induced redistribution of a chemical equilibrium, J. Am. Chem. Soc. 132 (45) (2010) 16107–16111.
[40] E. Yilgör, E. Burgaz, E. Yurtsever, İ. Yilgör, Comparison of hydrogen bonding in polydimethylsiloxane and polyether based urethane and urea copolymers, Polymer 41 (3) (2000) 849–857.
[41] T.-Y. Wei, T.-F. Chang, S.-Y. Lu, Y.-C. Chang, Preparation of monolithic silica aerogel of low thermal conductivity by ambient pressure drying, J. Am. Ceram. Soc. 90 (7) (2007) 2003–2007.
[42] F.S. Chuang, W.C. Tsen, Y.C. Shu, The effect of different siloxane chain-extenders on the thermal degradation and stability of segmented polyurethanes, Polym. Degrad. Stab. 84 (1) (2004) 69–77.
[43] J. Dutta, K. Naskar, Investigation of morphology, mechanical, dynamic mechanical and thermal behaviour of blends based on ethylene vinyl acetate (EVA) and thermoplastic polyurethane (TPU), RSC Adv 4 (105) (2014) 60831–60841.
[44] L. Shao, Z.-Y. Ji, J.-Z. Ma, C.-H. Xue, Z.-L. Ma, J. Zhang, The synergy of double cross-linking agents on the properties of styrene butadiene rubber foams, Sci. Rep. 6 (2016) 36931.
[45] J. Cho, I. Jeon, S.Y. Kim, S. Lim, J.Y. Jho, Improving dispersion and barrier properties of polyketone/graphene nanoplatelet composites via noncovalent functionalization using aminopyrene, ACS Appl. Mater. Interfaces 9 (33) (2017) 27984–27994.
[46] J. Yu, X. Huang, L. Wang, P. Peng, C. Wu, X. Wu, P. Jiang, Preparation of hyperbranched aromatic polyamide grafted nanoparticles for thermal properties reinforcement of epoxy composites, Polym. Chem. 2 (6) (2011) 1380–1388.
[47] B.J. Yang, J.-u. Jang, S.-H. Eem, S.Y. Kim, A probabilistic micromechanical modeling for electrical properties of nanocomposites with multi-walled carbon nanotube morphology, Composites, Part A 92 (2017) 108–117.
[48] S. Ravichandran, S. Nagarajan, B.C. Ku, B. Coughlin, T. Emrick, J. Kumar, R. Nagarajan, Halogen-free ultra-high flame retardant polymers through enzyme catalysis, Green Chem 14 (3) (2012) 819–824.
[49] H.-B. Chen, P. Shen, M.-J. Chen, H.-B. Zhao, D.A. Schiraldi, Highly efficient flame retardant polyurethane foam with alginate/clay aerogel coating, ACS Appl. Mater. Interfaces 8 (47) (2016) 32557–32564.